INSTITUTE OF PHYSICS PUBLISHING SMART MATERIALS AND STRUCTURES
Smart Mater. Struct. **12** (2003) 494–499 PII: S0964-1726(03)63340-9

Optimal location of collocated piezo-actuator/sensor combinations in spacecraft box structures

Christopher J Damaren

University of Toronto, Institute for Aerospace Studies, 4925 Dufferin Street, Toronto, ON M3H 5T6, Canada

E-mail: damaren@utias.utoronto.ca

Received 7 December 2001, in final form 10 April 2003
Published 30 May 2003
Online at stacks.iop.org/SMS/12/494

Abstract
The problem of actuator/sensor location is examined for the inclusion of piezoelectric smart structural elements in box-type structures. The box is modeled as a system of joined plates in which both extensional and bending deflections are incorporated. A location criterion is developed which is based on the damping injected into the first few modes by a simple constant gain feedback. It is found that the central regions of each face which avoid the edges and corners offer the most promising sites for collocating piezo-actuators and sensors.

1. Introduction

The application of layers of piezoelectric materials to thin-walled elastic structures offers the ability to introduce active damping in a distributed fashion [1]. By physically collocating such 'smart' materials configured as dual sensors and actuators the problem of spillover, the major problem in active vibration control, can be circumvented. However, the price paid for robustness is the potential loss of damping performance relative to the noncollocated situation. Hence, proper location of the collocated actuator/sensor site is important. Collocation has been exploited in controller design for smart structures by Pota *et al* [2].

Small satellites have been increasing in importance given the need to reduce spacecraft design costs. Reduction in size and mass while continuing to require tight performance objectives leads to active vibration control as a possible design alternative. Microspacecraft structures are typically simplistic in design and consist of homogeneous materials arranged in simple geometries. A box or stack of trays are common approaches.

Although many authors have looked at the control and/or location of smart structural elements in beam [3, 4] and plate structures [5–9], the box and tray-stack architectures have escaped notice. In addition to the small satellite application, this is a relatively simple structure with interesting but nontrivial vibration mode shapes. This article examines the optimal location of a collocated piezo-actuator/sensor combination in box-type structures.

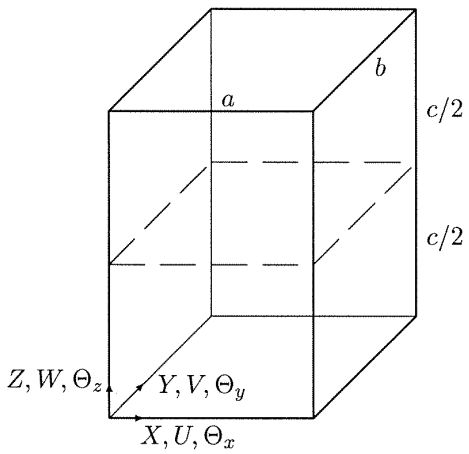

Figure 1. Box structure schematic.

2. Motion equations

A schematic of a box structure is shown in figure 1 along with the global axes $\{X, Y, Z\}$ and corresponding deflections $\{U, V, W\}$ and rotations $\{\Theta_x, \Theta_y, \Theta_z\}$. Each side of the box is modeled as a thin plate. We will also consider the inclusion of the dashed plate which we will term the tray-stack architecture.

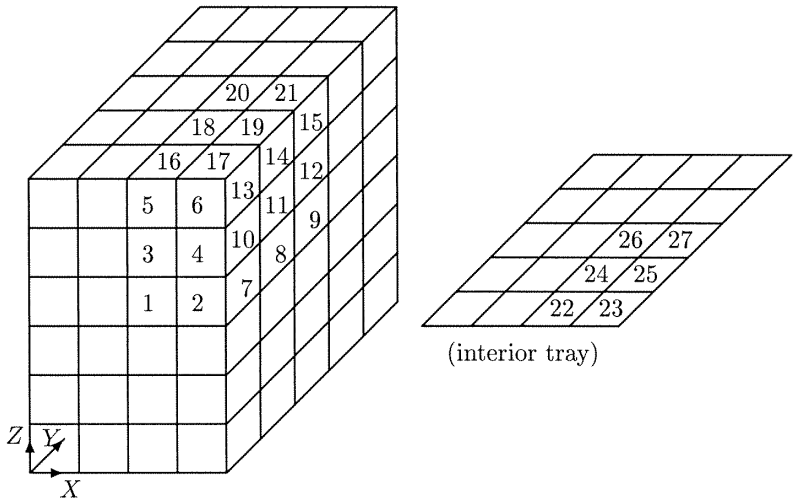

Figure 2. Sensor/actuator locations.

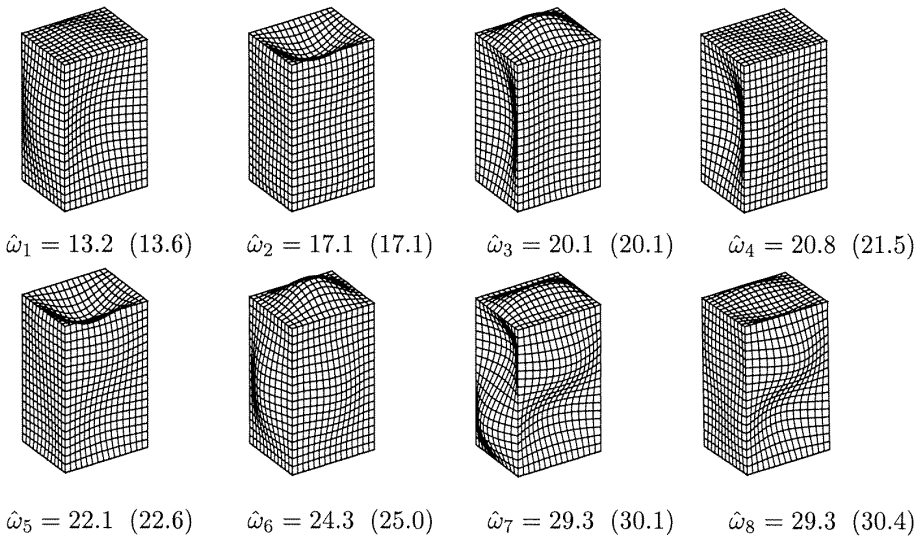

Figure 3. Box mode shapes.

A local coordinate frame is selected such that (x, y) lies in the plane of the plate and z is aligned with the surface normal. The x- and y-axes are parallel to the sides of the plate. The corresponding extensional deflections are $[u_0(x, y, t), v_0(x, y, t)]$ and the normal deflection is $w(x, y, t)$. For a homogeneous isotropic box of mass density ρ and panel thickness h, thin-plate theory gives the corresponding kinetic and potential energies for each plate as

$$T = \frac{1}{2}\rho h \int\int_S \left[\left(\frac{\partial u_0}{\partial t}\right)^2 + \left(\frac{\partial v_0}{\partial t}\right)^2 + \left(\frac{\partial w}{\partial t}\right)^2\right] \mathrm{d}x\,\mathrm{d}y \qquad (1)$$

$$\begin{aligned} V = {} & \frac{1}{2}D \int\int_S \left[\left(\frac{\partial^2 w}{\partial x^2}\right)^2 + \left(\frac{\partial^2 w}{\partial y^2}\right)^2 \right. \\ & \left. + 2\nu \frac{\partial^2 w}{\partial x^2}\frac{\partial^2 w}{\partial y^2} + 2(1-\nu)\left(\frac{\partial^2 w}{\partial x \partial y}\right)^2\right] \mathrm{d}x\,\mathrm{d}y \\ & + \frac{1}{2}C \int\int_S \left[\left(\frac{\partial u_0}{\partial x}\right)^2 + \left(\frac{\partial v_0}{\partial y}\right)^2 \right. \\ & \left. + 2\nu \frac{\partial u_0}{\partial x}\frac{\partial v_0}{\partial y} + \frac{1-\nu}{2}\left(\frac{\partial u_0}{\partial y} + \frac{\partial v_0}{\partial x}\right)^2\right] \mathrm{d}x\,\mathrm{d}y \end{aligned} \qquad (2)$$

where E is Young's modulus, ν is Poisson's ratio, $D = Eh^3/[12(1-\nu^2)]$ is the bending rigidity and $C = Eh/(1-\nu^2)$ is the extensional rigidity.

For spatial discretization, rectangular finite elements are used with the following expansions within each element:

$$u_0(\hat{x}, \hat{y}, t) = [\,1 \quad \hat{x} \quad \hat{y} \quad \hat{x}\hat{y}\,]\boldsymbol{A}_u \boldsymbol{q}_u(t) \qquad (3)$$

$$v_0(\hat{x}, \hat{y}, t) = [\,1 \quad \hat{x} \quad \hat{y} \quad \hat{x}\hat{y}\,]\boldsymbol{A}_v \boldsymbol{q}_v(t) \qquad (4)$$

$$\begin{aligned} w(\hat{x}, \hat{y}, t) = [\,1 \quad \hat{x} \quad \hat{y} \quad \hat{x}^2 \quad \hat{x}\hat{y} \quad \hat{y}^2 \quad \hat{x}^3 \quad \hat{x}^2\hat{y} \\ \hat{x}\hat{y}^2 \quad \hat{y}^3 \quad \hat{x}^3\hat{y} \quad \hat{x}\hat{y}^3\,]\boldsymbol{A}_w \boldsymbol{q}_w(t). \end{aligned} \qquad (5)$$

Here, $(\hat{x}, \hat{y}) \in [0, 1] \times [0, 1]$ are nondimensionalized local coordinates and $\boldsymbol{A}_u$, $\boldsymbol{A}_v$ and $\boldsymbol{A}_w$ are constant matrices evaluated so that $\boldsymbol{q}_u$, $\boldsymbol{q}_v$ and $\boldsymbol{q}_w$ contain prescribed nodal degrees of freedom at the element corners. In the case of $\boldsymbol{q}_u$ and $\boldsymbol{q}_v$ these are simply the four corresponding displacements, and in the case of $\boldsymbol{q}_w$ they are the corner values of $\{w, \partial w/\partial x, \partial w/\partial y\}$. The global vector of degrees of freedom, $\boldsymbol{q}$, contains the assembly of nodal degrees of

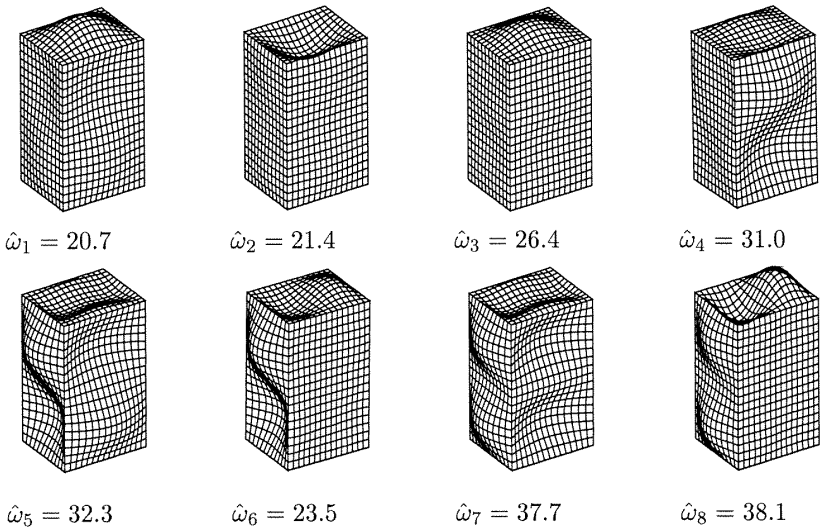

Figure 4. Tray-stack mode shapes.

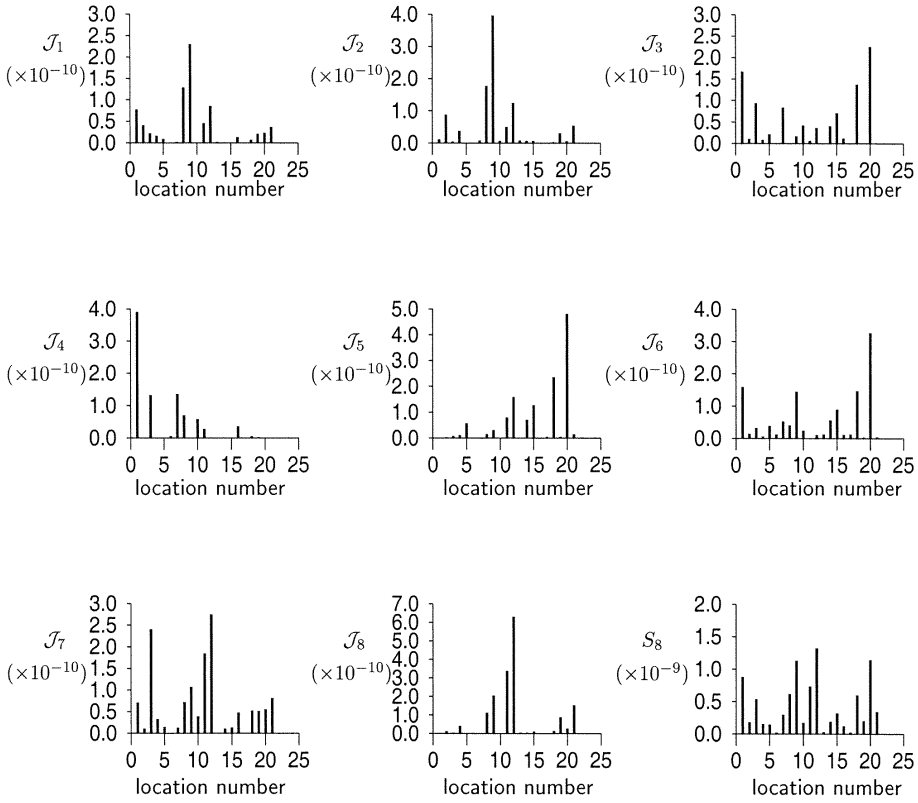

Figure 5. Box modal performance.

freedom which are the three displacements and rotations $\{U, V, W, \Theta_x, \Theta_y, \Theta_z\}$ and is readily constructed from simple transformations of $\boldsymbol{q}_u$, $\boldsymbol{q}_v$ and $\boldsymbol{q}_w$. With the above expansions, the energies take on the familiar forms $T = (1/2)\dot{\boldsymbol{q}}^{\mathrm{T}}\boldsymbol{M}\dot{\boldsymbol{q}}$ and $V = (1/2)\boldsymbol{q}^{\mathrm{T}}\boldsymbol{K}\boldsymbol{q}$ with symmetric matrices $\boldsymbol{M}$ and $\boldsymbol{K}$.

We assume that a single piezoelectric sensor is located on the structure whose area coincides with a single finite element. The locations to be considered are shown in figure 2 where symmetry has been exploited in reducing the number of possible locations. The corresponding piezo-actuator is collocated with it. It is assumed that the sensor and actuator are mounted on the same side of the plate and contribute negligible mass and stiffness.

Following [10], the current created by the piezo-sensor is $y(t) = \mathrm{d}q_s/\mathrm{d}t$ where the sensor charge is

$$q_s = \iint_S F(x, y) P_0(x, y) \left\{ \left[e_{31}^0 \frac{\partial u_0}{\partial x} + e_{32}^0 \frac{\partial v_0}{\partial y} \right] - z_k^0 \left[e_{31}^0 \frac{\partial^2 w}{\partial x^2} + e_{32}^0 \frac{\partial^2 w}{\partial y^2} \right] \right\} \mathrm{d}x\, \mathrm{d}y \tag{6}$$

where e_{31}^0 and e_{32}^0 are the piezoelectric charge constants, $F(x, y) = 1$ if (x, y) contains sensor electrodes and vanishes

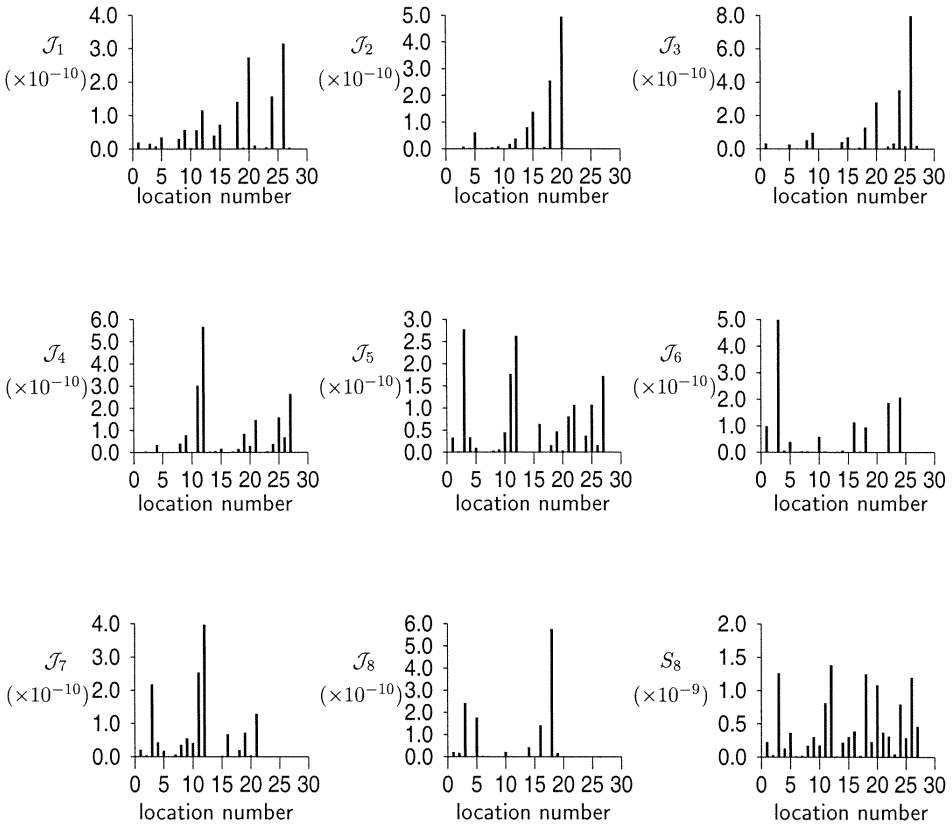

Figure 6. Tray-stack modal performance.

otherwise and $P_0(x, y)$ expresses the polarization profile which is taken to be identically unity here. The height of the layer above the plate's neutral axis is $z_k^0 = h/2$. Assuming uniform polarization within a rectangular patch area $S_p = [x_1, x_2] \times [y_1, y_2]$, we have

$$FP_0(x, y) = [H(x-x_1)-H(x-x_2)][H(y-y_1)-H(y-y_2)]$$

where $H(x)$ is the Heaviside step function. Substituting the expansions in equations (3)–(5) into (6) leads to the output equation

$$y(t) = \boldsymbol{c}^{\mathrm{T}}\dot{\boldsymbol{q}}$$

where $\boldsymbol{c}$ is a constant column vector.

The virtual work stemming from a collocated actuator is readily constructed from [10] as

$$\delta W_e = -\iint_S \delta_{ep} u(t) h_a \left[e_{31}^0 \frac{\partial (FP_0)}{\partial x}\delta u_0 + e_{32}^0 \frac{\partial (FP_0)}{\partial y}\delta v_0 + z_k^0 e_{31}^0 \frac{\partial^2 (FP_0)}{\partial x^2}\delta w + z_k^0 e_{32}^0 \frac{\partial^2 (FP_0)}{\partial y^2}\delta w \right] \mathrm{d}x\,\mathrm{d}y \qquad (7)$$

where h_a is the thickness of the actuator patch, $u(t)$ is the applied voltage and $\delta_{ep} = 1$ if the electric field and poling direction point in the same direction. Substituting the expansion equations (3)–(5) into the above and recognizing the duality between equations (6) and (7) leads to $\delta W_e = \delta \boldsymbol{q}^{\mathrm{T}} \boldsymbol{b} u(t)$ where $\boldsymbol{b} = h_a \boldsymbol{c}$. Applying Hamilton's principle to the energy and work expressions leads to the standard motion equations

$$\boldsymbol{M}\ddot{\boldsymbol{q}} + \boldsymbol{K}\boldsymbol{q} = \boldsymbol{b}u(t). \qquad (8)$$

It is readily apparent that the collocated rate feedback $u(t) = -ky(t)$ leads to the introduction of a symmetric damping term $kh_a \boldsymbol{c}\boldsymbol{c}^{\mathrm{T}}\dot{\boldsymbol{q}}$.

3. Modal analysis

The eigenproblem corresponding to (8) is

$$-\omega_\alpha^2 \boldsymbol{M}\boldsymbol{q}_\alpha + \boldsymbol{K}\boldsymbol{q}_\alpha = \boldsymbol{0}, \qquad \alpha = 1, 2, 3, \ldots$$

where ω_α are the undamped vibration frequencies with corresponding eigenvectors $\boldsymbol{q}_\alpha$ normalized so that $\boldsymbol{q}_\alpha^{\mathrm{T}} \boldsymbol{M} \boldsymbol{q}_\beta = \delta_{\alpha\beta}$. There are also zero-frequency rigid-body modes which are neglected in the subsequent analysis. Note that they are uncontrollable and unobservable given our choice of actuator and sensor. The modal expansion $\boldsymbol{q}(t) = \sum_\alpha \boldsymbol{q}_\alpha \eta_\alpha(t)$ introduced into (8) leads to uncoupled motion equations of the form

$$\ddot{\eta}_\alpha + \omega_\alpha^2 \eta_\alpha = b_\alpha u(t), \qquad b_\alpha = \boldsymbol{q}_\alpha^{\mathrm{T}} \boldsymbol{b}, \alpha = 1, 2, 3, \ldots \qquad (9)$$

with output $y(t) = \sum_\alpha c_\alpha \dot{\eta}_\alpha$ where $c_\alpha = h_a^{-1} b_\alpha$. For small k, the output feedback leads to the introduction of a small damping term $2\zeta_\alpha \omega_\alpha \dot{\eta}_\alpha$ on the left-hand side of each modal equation where the damping ratios are given by

$$\zeta_\alpha = \frac{kh_a}{2}\frac{c_\alpha^2}{\omega_\alpha}.$$

This expression clearly shows that the problem of actuator/sensor location resides in maximizing $|c_\alpha|$ for as many modes as possible.

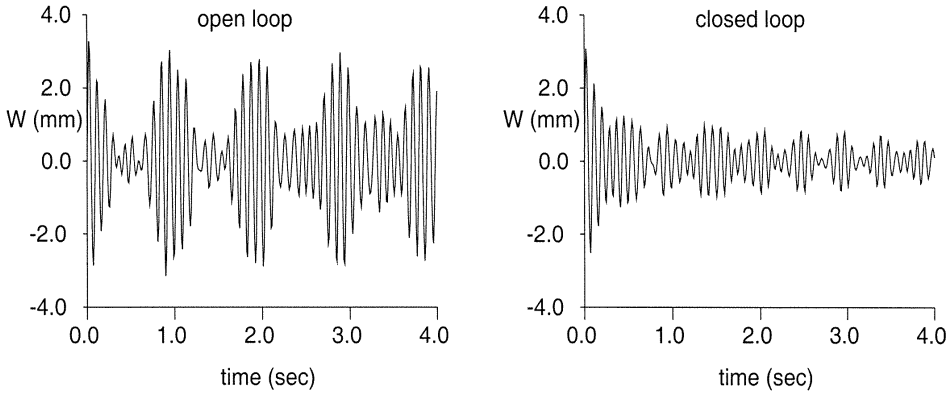

Figure 7. Box response to an impulsive force.

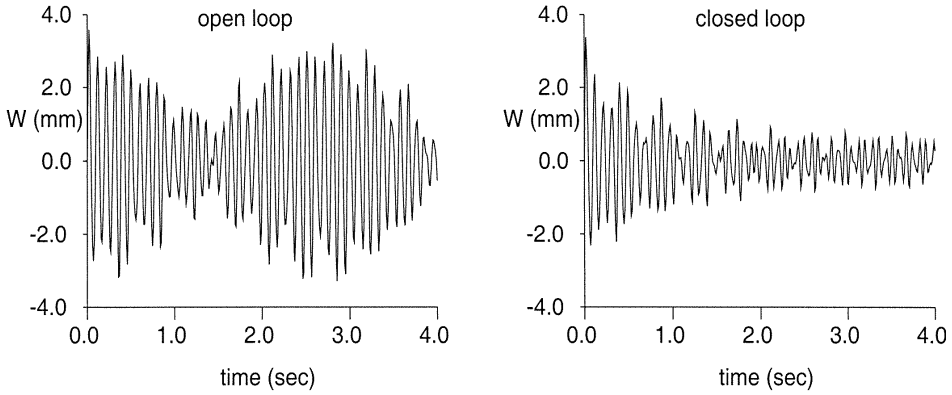

Figure 8. Tray-stack response to an impulsive force.

Before proceeding with this analysis, we illustrate the first eight vibration mode shapes (neglecting the six rigid-body modes) in figure 3 for a box with dimensions $a \times b \times c$ with $b/a = 1.25$ and $c/a = 1.5$. The vibration frequencies are also given with nondimensionalization $\hat{\omega}_\alpha^2 = \omega_\alpha^2 \rho h a^4 / D$. The numbers of finite elements in the X, Y and Z directions are four, five and six, respectively, which leads to square elements of identical size. The symmetries of the modes show good agreement with [11]. The experimentally determined frequencies of Dickinson and Warburton [12] for a steel box with the same aspect ratios as our example are also given in figure 3 (the bracketed quantities) and exhibit good agreement. The lack of complete localization of the mode shapes suggests that control authority over all displayed modes should be possible with a single actuator/sensor combination. The modes and frequencies for the tray-stack architecture (the interior plate shown in figure 1 is included) are shown in figure 4.

4. Optimal location analysis

Based on the previous section, the following performance measure is adopted for location optimization:

$$S_N = \sum_{\alpha=1}^{N} \mathcal{J}_\alpha, \qquad \mathcal{J}_\alpha = \frac{\hat{c}_\alpha^2}{\hat{\omega}_\alpha}, \qquad \hat{c}_\alpha = c_\alpha a^2 / [(e_{31}^0 + e_{32}^0)\sqrt{m}] \tag{10}$$

where m is the mass of the structure. We take $e_{31}^0 = e_{32}^0$ in the present study but the ratio of the two is fodder for further optimization studies. It is assumed that the actuator/sensor patch has dimensions $a/4 \times a/4$ and coincides with the domain of a finite element. This represents an obvious loss in generality but greatly simplifies the calculation of the c_α quantities and reduces the problem of optimal location to a discrete enumeration of a relatively small number of quantities. Given the symmetry of the structure, we only consider the locations explicitly numbered in figure 2.

The values of $\mathcal{J}_\alpha$ as a function of actuator/sensor location are shown for the first eight modes in figure 5 for the box structure. Location 9 maximizes this quantity for the first two modes and would clearly be the best choice if one wanted to damp only these two modes. Location 12 maximizes $\mathcal{J}_\alpha$ for modes 7 and 8 and location 20 maximizes this quantity for modes 3, 5 and 6. As an overall measure, we have selected S_8, which is also depicted in figure 5 as a function of location. Locations 9, 12 and 20 yield similar values of this measure but 12 is best. It is interesting to note that each of these locations avoids the edges and corners of the constituent plates.

The corresponding results for the tray-stack architecture are given in figure 6. Location 26 located on the interior tray optimizes modes 1 and 3. Location 12 optimizes modes 4 and 6 and location 3 is best for modes 5 and 6. The value of S_8 is very similar for these three locations as well as locations 18 and 20 but location 12 is again the best overall location. As with the box, all of these favorable sites avoid the edges and corners.

In an effort to illustrate the performance achieved using the optimal location, we consider an aluminum box ($E = 68$ GPa, $\rho = 2712$ kg m^{-3}, $\nu = 0.33$) with dimensions $a \times b \times c = 1$ m $\times$ 1.25 m $\times$ 1.5 m and a thickness of $t = 2$ mm. The properties of the piezoelectric material are $e_{31}^0 = e_{32}^0 = 0.06$ N m^{-1} V^{-1} and $h_a = 30 \times 10^{-6}$ m. For the closed-loop case, the feedback gain is set at 8×10^{14} V A^{-1}.

The box is initially quiescent and subject to an impulsive force located at the node shared by elements 18, 19, 20 and 21 in figure 2. The magnitude of the force is 1 N and it is directed in the positive Z direction. This is equivalent to a distribution of initial conditions for the modal coordinate rates, $\dot{\eta}_\alpha(0)$. The corresponding deflection of the box (neglecting the ensuing rigid-body motion) in the same direction at the same location is denoted by W. Both the open- and closed-loop responses are illustrated in figure 7 for the box and in figure 8 for the tray-stack. The damping injected by the feedback controller is clearly in evidence in both cases.

5. Concluding remarks

We have developed a finite element model of a box-type structure and used it to develop the modal properties and input–output characteristics for a collocated piezo-actuator/sensor combination. A measure of the damping injected into each mode by a simple constant gain feedback was used as a basis for optimizing the sensor/actuator location. It was found that good locations avoided the edges and corners of the box. Simulation results demonstrated the efficacy of the optimal location.

References

[1] Crawley E F and de Luis J 1987 Use of piezoelectric actuators as elements of intelligent structures *AIAA J.* **25** 1373–85

[2] Pota H R, Moheimani S O R and Smith M 2002 Resonant controllers for smart structures *Smart Mater. Struct.* **11** 1–8

[3] Bailey T and Hubbard J E Jr 1985 Distributed piezoelectric-polymer active vibration control of a cantilever beam *J. Guid. Control Dyn.* **8** 605–11

[4] Halim D and Moheimani S O R 2002 Experimental implementation of spatial H-infinity control of a cantilever beam *IEEE/ASME Trans. Mechatron.* **7** 346–56

[5] Baz A and Ro J 1996 Vibration control of plates with active constrained layer damping *Smart Mater. Struct.* **5** 272–80

[6] Wang S Y, Quek S T and Ang K K 2001 Vibration control of smart piezoelectric composite plates *Smart Mater. Struct.* **10** 637–44

[7] Sun D C, Tong L Y and Wang D J 2001 Vibration control of plates using discretely distributed piezoelectric quasi-modal actuators/sensors *AIAA J.* **39** 1766–72

[8] Han J H and Lee I 1999 Optimal placement of piezoelectric sensors and actuators for vibration control of a composite plate using genetic algorithms *Smart Mater. Struct.* **8** 257–67

[9] Halim D and Moheimani S O R 2003 An optimization approach to optimal placement of collocated piezoelectric actuators and sensors on a thin plate *Mechatronics* **13** 27–47

[10] Lee C K 1990 Theory of laminated piezoelectric plates for the design of distributed sensors/actuators. Part I: governing equations and reciprocal relationships *J. Acoust. Soc. Am.* **87** 1144–58

[11] Hooker R J and O'Brien D J 1974 Natural frequencies of box-type structures by a finite-element method *J. Appl. Mech.* **41** 363–5

[12] Dickinson S M and Warburton G B 1967 Vibration of box-type structures *J. Mech. Eng. Sci.* **9** 325